

# A Tchebycheff-based Multi-objective Combined with a PSO-SQP Dynamic Real-time Optimization Framework for Cycling Energy Systems

Rebecca Kim and Fernando V. Lima\*

*Department of Chemical and Biomedical Engineering, West Virginia University,  
P.O. Box 6102, Morgantown, WV 26506*

## Abstract

The aim in this work is to develop an optimization framework to address cycling of baseload energy systems due to the penetration of renewables into the grid. The developed strategy corresponds to a multi-objective and dynamic real-time optimization (MOO-DRTO) framework applied to a postcombustion MEA-based CO<sub>2</sub> capture process from a baseload coal-fired power plant under cycling conditions. A Tchebycheff-based method is used for the multi-objective optimization (MOO) component. Also, a hybrid approach consisting of Particle Swarm Optimization (PSO) and Sequential Quadratic Programming (SQP) is implemented for the first time in process systems engineering to solve the dynamic real-time optimization (DRTO) component. The objectives considered in the MOO-DRTO framework are economic and environmental. The proposed MOO-DRTO strategy is successfully implemented and 24-hour optimal output trajectories for the carbon capture system under cycling are generated. Also, the optimal compromise is chosen from the Pareto front according to a set of selected weights for the objectives with minimal interaction between the framework and decision maker. The results indicated that the developed framework has potential to be extended to plant-wide optimization applications under cycling.

## Keywords

*Dynamic optimization, carbon capture system, fossil-fueled power plant, renewable intermittency, PSO-SQP hybrid, nonlinear system*

\* Corresponding author

E-mail address: [Fernando.Lima@mail.wvu.edu](mailto:Fernando.Lima@mail.wvu.edu)

## 1. Introduction and Prior Work

Recent studies<sup>(1)-(3)</sup> forecast for the near future a fast and steady increase in the participation of renewable energy sources in the electricity generation mix. Power generation by intermittent renewables such as solar and wind has negligible costs regarding fuel and variable operation and maintenance costs, as well as, no emissions during electricity production. Most of the costs are related to the technology investment, construction and land of the power plant<sup>(2),(4)</sup>. Hence, it is advantageous to utilize the electricity generated by the renewables when available. Projections<sup>(1)</sup> show that the increase in the penetration of renewables into the grid is mainly due to higher utilization of solar and wind energy sources, which are becoming more cost competitive with solar costs falling 85% and wind costs falling 36% between 2008 and 2016<sup>(5)</sup>. However, due to the intermittency of the solar and wind energy sources, it is expected that the grid will have dispatchable energy sources available to always maintain the reliability and supply the demand load. Several strategies can be used to achieve this goal including the design of power plants considering flexible operations or use of large-scale batteries for energy storage. But the strategy being employed nowadays is to cycle the load of the already installed baseload power plants such as coal-fired (CFPP) and natural gas power plants (NGPP)<sup>(6)-(7)</sup>.

Imposing cycling on baseload power plants may introduce inefficiencies to the systems as they are no longer operating at their optimal design points. For instance, boilers are tuned to combust the coal at a specific rate and temperature and the emission control equipment is synchronized to operate with maximum efficiency at the design rate of the boiler. Thus, when the boiler is not operated consistently at the designed temperature, the resulting variability may cause problems with the way the boiler interact with the emission control units, which may lead to erratic emission behavior that can last for several hours before control is fully regained<sup>(6)</sup>. Also, in general, an increase in ramping up/down and

startup/shutdown frequency for the plant decreases the component life through damage caused by creep, fatigue, thermal shock, acid-induced corrosion, erosion, and other stresses<sup>(7)</sup>. Consequently, challenges related to loss of power plant efficiency, emissions control and increase of wear and tear are expected to arise as the fossil-fueled power plants cycle their load to accommodate solar/wind penetrations. To address these challenges, an optimization-based framework is proposed in this work so that the fossil-fueled power plants can comply with the demand load required, as shown in Figure 1. In summary, there are information flows between demand load, energy available from the fossil and renewable sources as well as potentially other forcing functions, such as market price or policies, with the optimizer. Then, the optimal operation of dispatchable energy sources are determined to supply the net demand load at all times. As there is a time constraint for online implementation, the dispatchable energy sources, such as CFPP, represented by the supercritical pulverized coal-fired power plant (SCPC) in Figure 1, NGPP or energy storage, are simulated in the optimizer using reduced-order models. This paper focuses on the optimization of an SCPC subsystem under cycling conditions, as an element of the overall framework proposed in Figure 1. In addition to the single baseload process optimization being performed in this paper, the overall framework will address in future work how different energy systems, such as baseload and load-following power plants, energy storage technologies and variable renewable energy sources would be optimally integrated to supply the demand.

The optimization approach should be implemented according to the timescales of the power system operations. In the unit commitment level, operation planners will turn on enough units to meet the forecasted demand, usually between six hours and a few days ahead. Throughout the day, traders will usually determine the electricity price based on a bid system while operators will give hourly schedules to units. As real-time approaches, operators adjust generator schedules to meet the quickly

changing demand. This is often referred to as load-following and units with sufficient ramping capabilities are used to meet demand on a five-minute to one-hour time basis<sup>(8)</sup>.

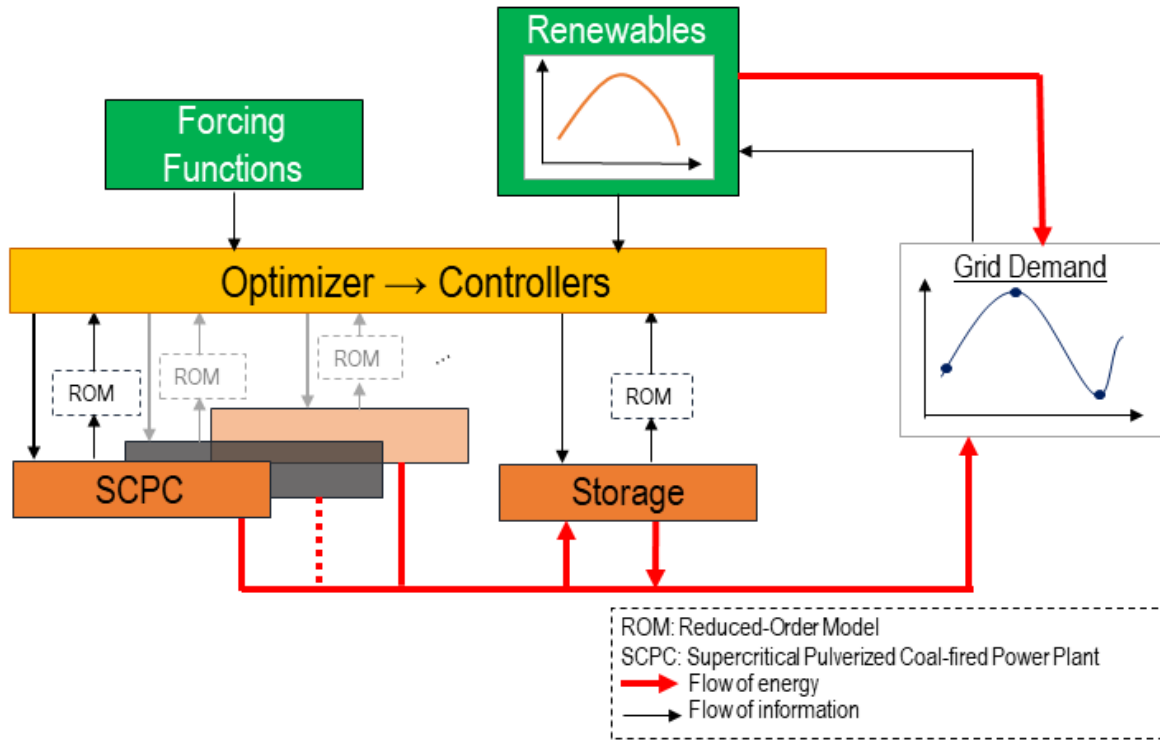


Figure 1 – Schematic of the optimization framework considering the SCPC with intermittent renewables

Typically, in the power plant optimization field, optimization techniques are performed to improve the steady-state behavior of the system, considering that the system dynamics can be neglected. This assumption simplifies the problem formulation resulting in less computational time to find an optimum when compared to the same problem size that accounts for time dependency. When this premise is not adopted, nonlinear partial differential equations are frequently required<sup>(9)-(10)</sup>, which may introduce additional challenges into the problem. For instance, the optimization may be limited by the size of the system due to the time-consuming task to write, validate and solve the models. Also, larger systems may lead to computational intractability and there is always the timeframe

constraint that needs to be considered when implementing the optimal trajectories in a load-following scenario. Although there are challenges related to dynamic optimization, process systems research on dynamic real-time optimization (DRTO) and control has become more and more active in recent years aiming to maintain the competitiveness of chemical plants even during transient events, as such events may lead to suboptimal operation and potential losses regarding economics, environmental and other goals<sup>(10)-(11)</sup>.

Previous work<sup>(10)</sup> of a DRTO and control of a hybrid small-scale energy system concluded that the DRTO layer added a proactive feature to the overall control architecture with high level of flexibility to integrate operational, economic and safety objectives. The same work motivated how larger energy systems hubs could be benefitted from a DRTO layer on top of the controllers. Moreover, reported research<sup>(10),(12),(13)</sup> performed on power plants or subsystems of the power plant considering renewables intermittency usually focuses on only one objective, typically economic. The main issue on overlooking other objectives to promote only the economic objective is that the optimal operation would be narrowly defined using one of the several factors that are critical to the system. Moreover, the potential opportunity of establishing an optimal policy that considers other objectives would be neglected. In some cases, the environment aspect is considered as part of a single objective with no guarantee that the optimal solution is a Pareto-optimal point<sup>(10)</sup>, or assessed using a sensitivity study<sup>(12)</sup>, or set as a constraint<sup>(13)</sup>. By employing the aforementioned valid methods, there is no guarantee that an optimal compromise, i.e., Pareto-optimal point, between the conflicting objectives would be reached. However, as pointed out by the 2018 Intergovernmental Panel on Climate Change (IPCC) report<sup>(14)</sup>, there is a need to reduce significantly the amount of anthropogenic greenhouse gases, such as the carbon dioxide, in the atmosphere to minimize the potential impacts correlated with

the rise of global mean surface temperature. Thus, the environmental performance is a critical component that should be considered as a separate objective.

In this context, in which it is desired to utilize the renewables when available, while maintaining the reliability of the grid by relying on cycling baseload power plants, the optimization framework in Figure 1 is motivated. In this work, an optimization approach is developed and applied to a baseload process under cycling conditions. The chosen application is the aqueous monoethanolamine (MEA)-based postcombustion carbon capture unit, as a subsystem of a SCPC<sup>(15)</sup>. This application was chosen as the SCPC is one of the most efficient coal-fired technologies originally designed to be operated in a baseload manner. Nowadays, the subcritical coal-fired power plants are heavily cycled; however, there is a rising industrial interest in the development of process systems strategies for SCPC cycling. Economic and environmental objectives are considered to optimally operate the dynamic system. The determined optimal output trajectories can ultimately be sent to lower-level advanced model-based controllers<sup>(16)-(17)</sup>.

The proposed method addresses the potential impacts of cycling of the carbon capture system (CCS) from the chemical plant perspective. The approach consists of a multi-objective and dynamic real-time optimization (MOO-DRTO) framework. For the DRTO component, a Particle Swarm Optimization (PSO) and Sequential Quadratic Programming (SQP) hybrid algorithm is employed to solve a dynamic programming problem under the time constraint. Regarding the multi-objective optimization (MOO) component, it consists of a Tchebycheff-based weighted metric method to guarantee a Pareto-front optimum that is solved by an SQP algorithm. The overall framework using a PSO-SQP hybrid method to solve the DRTO component and the Tchebycheff-based MOO component is employed for the first time in the Process Systems Engineering (PSE) field.

This paper is organized as follows. In Section 2, the optimization background is briefly given for the DRTO and MOO components of the optimizer. The proposed optimization approach of the hybrid PSO with SQP are then presented in Section 3. The implementation of the proposed optimizer on the CCS under cycling considering different carbon capture scenarios are discussed in Section 4. Finally, the paper conclusions and future work are summarized in Section 5.

## 2. Optimization Preliminaries

In this section, the general mathematical background on the optimization techniques considered is provided to assist the understanding of the subsequent sections.

### 2.1. Dynamic Real-time Optimization (DRTO)

The general DRTO formulation considered here is defined in Equations (1) – (4):

$$\min_x \Phi(x, t) \quad (1)$$

subject to:

$$\frac{dx}{dt} = f(x, t) \quad g(x, t) = 0 \quad h(x, t) \leq 0 \quad (2) - (4)$$

in which,  $\Phi$  is the objective function to be minimized,  $f$  is the dynamic model that describes the system,  $g$  are the equality constraints,  $h$  are the inequality constraints,  $x(t)$  are the decision variables, and  $t$  is the time.

The main difference in the DRTO formulation when compared to a typical steady-state linear or nonlinear optimization problem is that the time dependency of the decision variables is considered during the calculations. As the objective function and the constraints are dependent on time, the optimal solution also changes over time. For instance, in the cycling scenario, electricity price and energy demand change with time, which cause the optimal operation of a power plant or subsystem

of the power plant also vary with time. Thus, flexibility is added to the operation when a dynamic component is incorporated into the optimizer, as the optimum during transient states can be tracked.

In this work, the optimal trajectories are determined using dynamic programming considering the maximum principle and Bellman's principle of optimality. The principle of optimality states that the minimum or maximum value of a function is dependent on the initial state and the initial time<sup>(18)</sup>. Thus, the overall problem can be divided into subproblems in which a decision can be made and the optimum trajectory up to time  $T$  is determined by the initial state  $t_0$ .  $T$  is considered the time of the overall problem and  $t_0$  the initial time of the problem. For instance, considering  $T = 10\text{h}$  and  $t_1 = 0.5\text{h}$ , the dynamic programming is composed of 20 subproblems each of 0.5h time length.

## 2.2. Multi-objective Optimization (MOO)

Simply stated, optimization can be defined as minimization or maximization of one (single objective) or more objectives (multi-objective) that are functions of real and integer variables, while satisfying the problem constraints. A MOO method is recommended when the problem has more than one objective that should be considered during the optimal search and the trade-off between objectives is not straightforward. For a well-posed MOO, the objectives are conflicting, i.e., one objective cannot be optimized without affecting the optimal solution of at least one other objective.

Considering a multi-objective optimization problem, the definition of the objective function  $\Phi$  can be extended to Equation (5):

$$\min_x \Phi(x), \text{ in which } \Phi(x) = [\Phi_1, \dots, \Phi_k] \quad (5)$$

in which  $k \geq 2$  denotes the number of objective functions. Due to the existence of several objective functions, the concept of optimality changes. The aim in a MOO problem is to find optimal compromises among objectives rather than an optimal solution corresponding to a single objective.

The optimality of a MOO problem is defined using the dominance and non-dominance concepts. A solution  $x_1$  is said to dominate  $x_2$  if and only if  $\Phi_i(x_1) \leq \Phi_i(x_2)$  for all  $i = 1, \dots, k$  and  $\Phi_i(x_1) < \Phi_i(x_2)$  for at least one of  $i \in \{1, \dots, k\}$ . If strict inequality holds for all  $k$  components, then  $x_1$  strictly dominates  $x_2$ , as expressed in Definitions 1 and 2 below:

Definition 1:  $x_1$  dominates  $x_2 \Leftrightarrow \Phi_i(x_1) \leq \Phi_i(x_2) \forall i \in \{1, \dots, k\}$  and  $\exists i : \Phi_i(x_1) < \Phi_i(x_2)$

Definition 2:  $x_1$  strictly dominates  $x_2 \Leftrightarrow \Phi_i(x_1) < \Phi_i(x_2) \forall i = 1, \dots, k$

A solution  $x_1$  is said to be a Pareto optimal solution if and only if there is no  $x_2$  that dominates  $x_1$  for  $i \in \{1, \dots, k\}$ . If there is no feasible solution that strictly dominates  $x_1$ , then  $x_1$  is called a weak Pareto optimal solution, as expressed in Definitions 3 and 4:

Definition 3:  $x_1$  is a Pareto optimal solution  $\Leftrightarrow \nexists x_2 : \Phi_i(x_2) < \Phi_i(x_1) \forall i \in \{1, \dots, k\}$

Definition 4:  $x_1$  is a weak Pareto optimal solution  $\Leftrightarrow \nexists x_2 : \Phi_i(x_2) \leq \Phi_i(x_1) \forall i \in \{1, \dots, k\}$

Pareto optimality is defined with respect to the entire decision variable space, unless otherwise specified. In other words,  $x_1$  is considered Pareto optimal if there exists no feasible decision vector within the set which would decrease some objective without causing a simultaneous increase in at least one other objective, in a minimization formulation.

The Pareto optimal set is a set of decision vectors that satisfy Definitions 3 and 4, i.e., the set is composed of non-dominated solutions of Definitions 3 and 4. The mapping of the decision vectors in the Pareto optimal set to the objective space creates a set of objective vectors, as defined by Equation (5), denominated as the Pareto optimal front or the non-dominated Pareto-front<sup>(19)</sup>.

### 3. Proposed Approach: Tchebycheff-based Multi-objective and Dynamic Real-time Optimization with PSO/SQP Hybrid Framework (MOO-DRTO)

The proposed approach to optimize a designed baseload process under renewables intermittency and different objectives is composed of multi-objective and dynamic real-time optimization elements. The DRTO optimizes the process considering the dynamics of the baseload system during cycling and the MOO chooses the optimal compromise between different objectives with respect to the optimization performed by the DRTO. The MOO component is based on a modified Tchebycheff weighted metric method and solved using a Sequential Quadratic Programming (SQP) algorithm, whereas the DRTO component is solved using a hybrid of Particle Swarm Optimization (PSO) and SQP algorithms.

Specifically, the PSO is used to find the best estimate for the initial guess of the SQP, and then the SQP determines the optimal trajectory for each objective. As the process addressed is nonlinear and it does not have strict convexity properties, the solution found by the SQP that satisfies the optimality conditions will be the closest local optimum to the provided initial guess. Therefore, it is always advantageous for these problems to have a good initial guess. A systematic method for defining the initial guess for the SQP using PSO is established without relying on privileged knowledge of the system. PSO is a meta-heuristic method inspired by the nature social behavior and dynamic movements with communication of groups such as insects, birds, and fishes. PSO is composed of decentralized entities with lower-level goals with no perception of higher-level goals but with capabilities to model complex real-world systems<sup>(20)</sup>. Each particle in the swarm is a potential solution

and it is influenced by experiences of the neighboring particles as well as its own experience. In this work, a global topology is adopted, i.e., each particle communicates with the entire swarm.

The PSO formulation considers how the particles move within a swarm and communicate to locate an optimum in the feasible space. Over time, through the combination of exploration and exploitation of known positions in the search space, the particles cluster or converge together around an optimum<sup>(20)</sup>. Through exploration, the particles search new regions of the feasible space whereas through exploitation the particles attempt to improve or benefit from the known promising regions. After the positions and velocities of each particle are initialized, the position of each particle in the next time step is updated recursively, as it is shown in Equations (6) and (7)<sup>(21)</sup>:

$$v_j(t + 1) = IT * v_j(t) + c_1 * r_1 * (PB_j - p_j(t)) + c_2 * r_2 * (SB - p_j(t)) \quad (6)$$

$$p_j(t + 1) = p_j(t) + v_j(t + 1) \quad (7)$$

in which  $p_j$  is the position of the  $j$ -th particle,  $v_j$  is the velocity of the  $j$ -th particle,  $PB_j$  is the personal best position of the  $j$ -th particle,  $SB$  is swarm best position,  $IT$  is the inertia term,  $c_1$  and  $c_2$  are cognitive and social acceleration coefficients, and  $r_1$  and  $r_2$  are random numbers between  $[0,1]$ . The terms  $IT$ ,  $c_1$ , and  $c_2$  are determined using the constriction factor method. This method was developed from eigenvalue analysis of computational swarm dynamics, as described in Equations (8) – (11)<sup>(21)</sup>:

$$IT = \frac{2\gamma}{|2 - \Omega - \sqrt{\Omega(\Omega - 4)}|}, \quad \gamma \in [0,1] \quad (8)$$

$$\Omega = \Omega_1 + \Omega_2, \quad \Omega \geq 4 \quad (9)$$

$$c_1 = IT * \Omega_1 \quad c_2 = IT * \Omega_2 \quad (10) - (11)$$

in which  $\Omega, \Omega_1, \Omega_2, \gamma$  are the constriction factors. Under this method, the swarm convergence is guaranteed with particles decelerating as iteration count increases. The parameter  $\gamma$  controls the local

or global convergence. When  $\gamma$  is set close to 1, particles traverse the search space with a predominant emphasis on exploration. When  $\gamma$  is close to 0 the convergence is fast, but the solution quality may vary vastly<sup>(21)</sup>.

Then after a certain number of iterations, the swarm best is sent to the SQP algorithm as initial guess for determination of the optimal trajectories. The SQP algorithm used is the one available in *fmincon* in MATLAB®, which essentially takes the user supplied initial guess and determines the local optima by solving quadratic subproblems within the constraint and optimality tolerances. A hybrid PSO and SQP approach has been previously adopted<sup>(22)</sup> to solve the dynamic economic emission dispatch problem considering valve-point effect from the electric grid perspective. However, the multi-objective optimization was solved by converting the objectives into a single objective using the weighted sum method, which does not necessarily guarantee that the Pareto optimal compromise is obtained. Also, this optimization was performed from the electric grid (not PSE) perspective, i.e., the dynamics of the power plant as a chemical process were not considered.

In this work, the MOO component is solved by using the Tchebycheff weighted metric method that decomposes the MOO problem into a set of scalar optimization problems. The conventional Tchebycheff (*Tch*) decomposition can be defined<sup>(23)</sup> as in Equation (12):

$$\min_{x \in F} Tch(\Phi(x)|w, z^0), \text{ in which } Tch = \max_{1 \leq i \leq k} \{w_i |\Phi_i(x) - z_i^0|\} \quad (12)$$

in which,  $w$  is a  $k$ -dimensional weight vector with  $\sum_{i=1}^k w_i = 1$  and  $w_i \geq 0$ ,  $z^0$  with  $z_i^0 \leq \min\{\Phi_i(x)|x \in F\}$  is an ideal vector, and  $F$  is the decision space of  $n$ -dimensional decision variables. The ideal vector contains the optimum for each separately considered objective achieved in  $F^{n(19)}$ . Equation (12) shows that the optimizer attempts to minimize the maximum distance between the compromise and the ideal point for the  $i$ -th objective. Thus, the optimal MOO compromise is

determined by a specific weight vector and the distance of the chosen Pareto point to the ideal vector. Figure 2 conceptually shows how changing the values of the weight vector  $w$  directs the search to different areas of the Pareto front. From a determined initial point and specified weight vector, the optimizer iteratively minimizes the maximum distance until it reaches the Pareto front and the objective cannot be further improved.

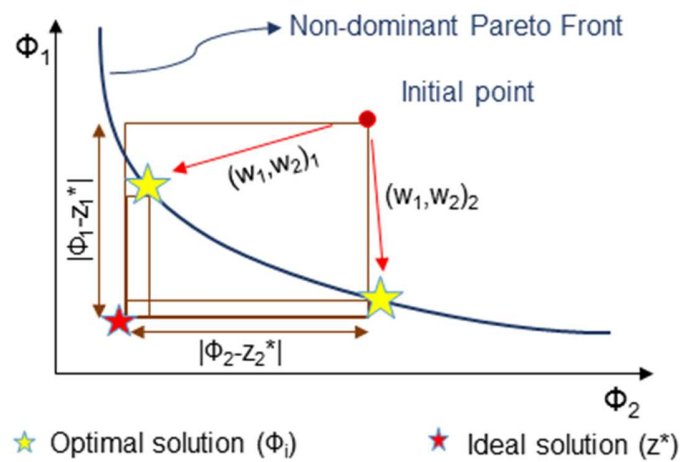


Figure 2 – Representation of the multi-objective optimization using the Tchebycheff optimal compromise considering different weights for two objectives

Thus, by inspection of Equation (12) and the representation in Figure 2, one can infer that every Pareto point is a solution of the Tchebycheff formulation by varying the weight vector. As a direct result, any Pareto optimal solution can be systematically found if the Tchebycheff metric is used, even for a non-convex Pareto-front. Therefore, any optimal compromise could be obtained in an online fashion, minimizing the interaction with the decision maker when compared to the traditional approach of first generating the Pareto front, and then selecting the optimal compromise. However, the solutions obtained by the conventional Tchebycheff decomposition method with uniform weights are not always uniformly distributed in the Pareto front. The modified Tchebycheff (*MTch*)

decomposition method was then proposed<sup>(23)</sup> to deal with this issue. The modified decomposition is constructed as seen in Equation (13):

$$\min_{x \in F} MTch(\Phi(x)|w, z^0) = \max_{1 \leq i \leq k} \left\{ \frac{\Phi_i(x) - z_i^0}{w_i} \right\} \quad (13)$$

in which the variables are defined similarly to Equation (12). Due to the property of Equation (13) to generate spatially uniformly distributed solutions in the Pareto front when weights are uniformly changed (i.e., the modified version avoids clustering behavior or high sensitivity to small changes on weights), as reported in the open literature<sup>(23)</sup>, the modified Tchebycheff method is adopted in this work when the weights are other than 0.

As presented in Equation (12), a  $w_i$  close to 1 has an intrinsic bias towards to the  $i$ -th objective. For the modified Tchebycheff as presented in Equation (13), a  $w_i$  close to 0 has an intrinsic bias towards to the  $i$ -th objective. Thus, aiming to have a cohesive method that spans throughout the weight vector values in a continuous manner, including when the weight is equal to zero, a slight modification is proposed in this work to Equation (12) to be used alongside Equation (13), as shown in Equation (14):

$$\min_{x \in F} Tch(\Phi(x)|w, z^0) = \max_{1 \leq i \leq k} \{(1 - w_i) |\Phi_i(x) - z_i^0|\} \quad (14)$$

such that a  $w_i$  close to 0 has an intrinsic bias towards to be closer to the  $i$ -th objective, same behavior seen in the modified Tchebycheff method shown in Equation (13). Further analysis shows that when weights 0 or 1 are inserted in Equation (14), the MOO fundamentally reduces to a single-objective optimization. The overall Tchebycheff-based method employed in this work is summarized below:

$$\min_{x \in F} MTch(\Phi(x)|w, z^0) = \max_{1 \leq i \leq k} \left\{ \frac{\Phi_i(x) - z_i^0}{w_i} \right\} \quad \text{for } 0 < w_i < 1 \quad (13)$$

$$\min_{x \in F} Tch(\Phi(x)|w, z^0) = \max_{1 \leq i \leq k} \{(1 - w_i) |\Phi_i(x) - z_i^0|\} \quad \text{for } w_i = 0; w_i = 1 \quad (14)$$

In this work, the weights attributed to each objective determine the initial guess to be supplied to the SQP of the MOO problem. If the bias is towards the  $i$ -th objective, the initial guess will be the one that optimizes the  $i$ -th objective. For instance, if weight vector is  $[0.1, 0.9]$ , the supplied initial guess for the MOO is the one that optimizes objective 1, as  $w_1 = 0.1$ .

For both *Tch/MTch* formulations, it is recommended for the objectives to be normalized, which requires the objectives to be bounded and known by the optimizer. In this work, the maximum and minimum, as well as the ideal vector for the MOO are obtained using the proposed hybrid DRTO approach based on PSO and SQP algorithms. Then the calculated trajectories, maximum, and minimum are sent to the MOO component to decide on the optimal compromise. Figure 3 outlines the proposed MOO-DRTO optimization algorithm for baseload systems under cycling conditions that consists of the nine steps described below:

Initialization: The dynamic system model and forcing functions, as well as the optimization time horizon  $T$ , the PSO parameters and the weight vector determined by the decision maker are sent to the optimizer to initialize the overall algorithm.

(i) The time is set to  $t = t_0$ , which refers to the initial time of the DRTO dynamic programming.

(ii) The PSO algorithm is initialized for a determined number of particles. The particles are randomly and uniformly distributed in the feasible space and random velocities are attributed to each particle. Then each particle stores its position as the particle best thus far. The swarm best is also assessed and stored.

(iii) After the PSO is initialized, each particle position and velocity are updated recursively using Equations (6) and (7) for a defined number of iterations. At each iteration, particle best and swarm

best are verified and updated if better objective values are reached considering the particle history/swarm history. Then the swarm best is sent to the SQP as initial guess.

(iv) The dynamic programming subproblem is solved by the SQP and the minimum and maximum of the objectives are determined. Then, the optimal trajectories from  $t$  to  $t+t_1$  for each objective are obtained. The minimum and maximum values of the subproblem are used to determine the ideal vector and to normalize the objectives of the MOO component.

(v) At every SQP iteration, the constraint, optimality, and step differences are checked to identify if they are lower than the tolerances stipulated for the algorithm:

1. If *yes*, the minimum, maximum, and optimal trajectories are sent to the MOO component;
2. If *no*, go back to step (iv) and perform another iteration until the criteria are satisfied.

(vi) At this point, depending on the weight vector previously determined by the decision maker, a suitable *Tch/MTch* formulation from Equations (13) and (14) and initial guess are used to determine the optimal compromise employing an SQP algorithm.

(vii) At every SQP iteration of the MOO, the constraint, optimality, and step differences are checked to identify if they are lower than the tolerances stipulated for the algorithm:

1. If *yes*, the trial point converged within the tolerances;
2. If *no*, go back to step (vi) and perform another iteration until the criteria is satisfied.

(viii) Implement the optimal trajectory on the dynamic system and update the time horizon  $t=t+t_1$ , in which  $t_1$  represents the time length of the DRTO subproblem solved.

(ix) Assess if all the DRTO subproblems were solved by checking if  $t = T$ :

1. If *yes*, exit the optimizer framework.
2. If *no*, then repeat steps (ii)-(ix) until the criterion  $t = T$  is satisfied.

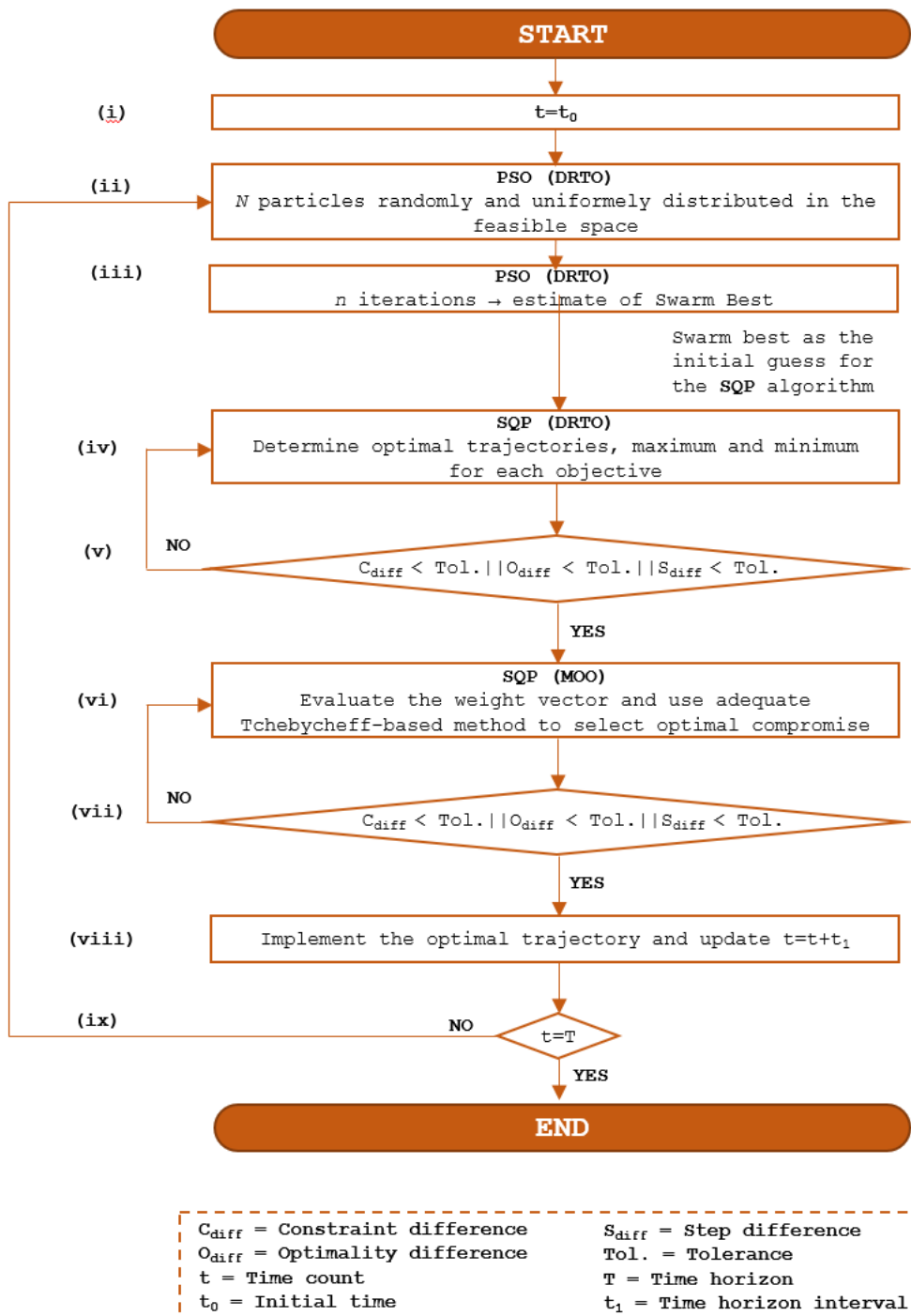


Figure 3 – Proposed optimization algorithm with dynamic programming and multi-objective optimization

#### 4. SCPC MEA-based CO<sub>2</sub> Capture Subsystem: Application and Results

The application addressed in this paper is the MEA-based carbon capture system (CCS) from a SCPC plant shown in Figure 4, originally designed to operate in baseload conditions. The system is composed of an absorber and stripper column system that uses a closed-loop circulating MEA solvent. Initially, a set of pumps and a direct contact cooler (DCC) are used to condition the flue gas coming from the SCPC plant. Then the conditioned flue gas is sent to the absorber where the CO<sub>2</sub> is absorbed into the MEA solvent and the cleaner flue gas is vented to the atmosphere with a lower CO<sub>2</sub> content. The MEA solvent rich in CO<sub>2</sub> goes to the stripper where the solvent is regenerated and lean MEA solvent is returned to the absorber. Whereas, the high-purity CO<sub>2</sub> may be stored or conditioned for other purposes, by pressurizing it using a multistage compressor to a suitable pressure. The energy penalty for CO<sub>2</sub> removal is significant as thermal energy must be provided to regenerate the solvent in the stripper reboiler, usually supplied by extracting low-pressure steam from the power plant, and due to the multistage compressor. The CCS model is a first-principles high-fidelity model in Aspen Dynamics®<sup>(15)</sup>. Column size and operational specifications of the CCS at the nominal point are shown Table 1.

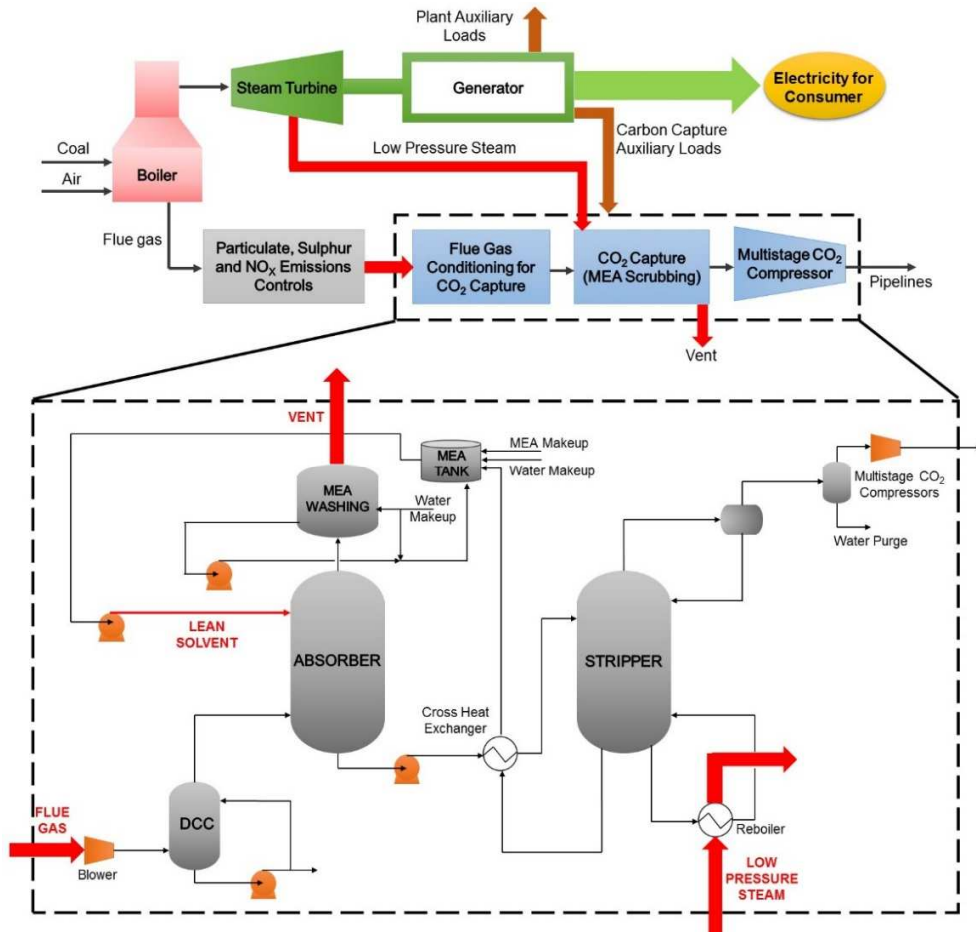


Figure 4 – Supercritical coal-fired power plant with the MEA-based carbon capture subsystem (CCS) in detail

Table 1 – SCPC operating conditions at nominal point and column size specifications<sup>(15)</sup>

<b>Parameters</b>	<b>Specification</b>
<b>Net power without carbon capture (kW)</b>	549,990
<b>Net plant efficiency without carbon capture (HHV)</b>	39.30%
<b>Net power with carbon capture (kW)</b>	420,251
Flue gas blower (kW)	3,237
CO <sub>2</sub> compressor (kW)	33,344
Rich solvent pump (kW)	178
Power loss on reboiler (kW)	92,980
<b>Net plant efficiency with carbon capture (HHV)</b>	30.03%
<b>Efficiency penalty due to carbon capture</b>	9.27%
<b>Flue gas temperature (K)</b>	310
<b>Lean solvent temperature (K)</b>	308
<b>Lean solvent loading (%)</b>	28.6
<b>Absorber pressure (bar)</b>	1.0
<b>Stripper pressure (bar)</b>	2.1
<b>Absorber height (m)</b>	24
<b>Absorber diameter (m)</b>	5.8
<b>Stripper height (m)</b>	24
<b>Stripper diameter (m)</b>	5.4
<b>MEA washing column height (m)</b>	2.4
<b>MEA washing column diameter (m)</b>	5.8

For the optimization problem definition, the flue gas, low-pressure steam, and lean solvent flowrates are considered as the decision variables, as highlighted in Figure 4, in which the flue gas flowrate has a constraint due to the assumed cycling profile; whereas total power consumption, lean solvent CO<sub>2</sub> loading and CO<sub>2</sub> capture rate are the dependent variables. The power consumption is assumed as the total power required for the CCS to operate and it refers to the power supplied to the blowers and compressors as well as the equivalent work associated with the thermal energy supplied to the stripper's reboiler. The CO<sub>2</sub> capture rate is calculated according to DOE/NETL in which the carbon capture rate is defined as one minus the amount of the carbon being released in the stack relative to the total carbon in the system<sup>(24)</sup> as given by Equation (15):

$$\text{CO}_2 \text{ capture rate} = 1 - \left( \frac{\text{CO}_2 \text{ in stack}}{\text{Total CO}_2 \text{ in}} \right) \quad (15)$$

The lean solvent CO<sub>2</sub> loading is defined in Equation (16):

$$\text{Lean solvent CO}_2 \text{ loading} = \frac{\text{CO}_2 \text{ flowrate on the top of stripper}}{\text{lean solvent back to the absorber}} \quad (16)$$

Based on carbon dioxide policy cases reported<sup>(25)</sup>, it is considered for the optimization studies the potential existence of carbon tax and *cap&trade* policies as well as an enhanced oil recovery (EOR) market for the captured carbon. Also, as the CCS in this work is a subsystem of the SCPC plant, it is assumed that: the CCS is already established and operating, which implies there is no additional capital costs associated with the unit; the power demand constraint is always satisfied; and the flue gas flowrate is a constrained decision variable for the CCS that cycles as needed to satisfy such power demand. The optimal trajectories are calculated considering a 1-hour ahead perfect forecast for the market and the power generated by the renewable energy sources.

First, for online optimization purposes, the order of the high-fidelity Aspen Dynamics® model is reduced to address potential computational tractability issues<sup>(26)</sup>. The reduced-order model is generated based on input-output simulated Aspen Dynamics® data and by employing system identification techniques. Then, the reduced-order model is provided along with the forcing functions to the MOO-DRTO framework. The optimal trajectories are then determined and can be sent, for instance, to advanced model-based controllers for implementation. The results regarding the system identification and optimization components of this framework are discussed separately below.

#### 4.1. System Identification

The system identification designed sequence for all decision variables (inputs) is based on pseudo-random binary signals (PRBS). Due to the deadtime in the response of the system to varying inputs of approximately 30 minutes, the PRBS test is designed to introduce step tests for each decision

variable every 1 hour, while the responses of the dependent variables (outputs) are recorded. The tests are performed with approximately 10% deviation around the steady-state (SS) value of each variable as shown in Equations (17) – (19):

$$\text{Fluegas flowrate } (x_1)_{SS} = 3.53 \text{ (kmol/s)} \quad 3.38 \leq x_1 \leq 3.69 \quad (17)$$

$$\text{Lean MEA solvent flowrate } (x_2)_{SS} = 10.09 \text{ (kmol/s)} \quad 9.65 \leq x_2 \leq 10.56 \quad (18)$$

$$\text{Low – pressure steam flowrate } (x_3)_{SS} = 1.40 \text{ (kmol/s)} \quad 1.35 \leq x_3 \leq 1.45 \quad (19)$$

The model structure is chosen by analyzing the generated input-output data. For this case study, the generated data indicated input-dependent stability and dynamic nonlinearity response to a time-varying input signal<sup>(27)</sup>. Thus, the Nonlinear AutoRegressive with eXogenous inputs (NARX) structure with wavelet networks is chosen, as this class can represent the observed behaviors. The input-output relationship given by a NARX structure is described by the nonlinear Equation (20) below:

$$y(t) = fc \left( y(t-1), \dots, y(t-n_y), x(t), x(t-1), \dots, x(t-n_u) \right) + \varepsilon(t) \quad (20)$$

in which  $fc$  is a nonlinear mapping,  $y$  are the dependent variables,  $x$  are the decision variables,  $\varepsilon$  is an independent identically distributed random variable, and  $n_y$  and  $n_u$  are the maximum input and output lags, respectively<sup>(28)</sup>. It is assumed that the nonlinear mapping  $fc$  can be characterized as a finite set of hierarchical correlated functions expanded in terms of the lagged output and input variables. For the identification task, wavelet networks are chosen to represent the nonlinear component.

The model selection is performed by analyzing the correlations of the residuals, the Akaike information criterion (AIC), the root mean square error (RMSE), and the match between the simulated data from the Aspen Dynamics® model with the 1-hour ahead model prediction. AIC and RMSE are statistics that measure the goodness of fit and it is desired to have a model with lower values for both statistics.

Each assessed model differs from each other by the number of predictor variables, i.e., regressors, employed for each selected output variable (carbon capture rate, lean solvent CO<sub>2</sub> loading, total equivalent work) and the time delay considered for the regressors. Table 2 shows the comparison between the statistics of candidate models analyzed. For all the models, the AIC and RMSE values are within the same order of magnitude. However, the performance regarding the 1-hour ahead prediction changes greatly among the models, with Model 9 being the one with the highest match within the assessed models with uncorrelated residuals. Based on the quality of the model predictions, Model 9 is selected as it can be used to reasonably forecast future output responses for specific inputs within the range of the identification data considered. The regressors and number of wavelet network units used for building Model 9 for each output are contained in Table 3.

Table 2 – AIC, RMSE and corresponding values for potential NARX models candidates

Parameters	AIC	RMSE	1-hour ahead prediction correspondence		
			Carbon Capture rate	Lean solvent CO <sub>2</sub> loading	Total equivalent work
<b>Model 0</b>	-1.01E-05	25.41	41.12%	81.57%	71.65%
<b>Model 1</b>	-1.04E-05	23.72	39.29%	79.47%	69.62%
<b>Model 2</b>	-1.02E-05	28.90	42.41%	80.35%	73.11%
<b>Model 3</b>	-1.03E-05	22.89	40.33%	77.44%	54.72%
<b>Model 4</b>	-1.30E-05	22.48	-7.62%	-62.74%	67.43%
<b>Model 5</b>	-1.13E-05	15.24	30.02%	-12.66%	65.12%
<b>Model 6</b>	-1.46E-05	15.19	34.54%	89.04%	80.16%
<b>Model 7</b>	-1.43E-05	15.19	-28.62%	76.53%	77.04%
<b>Model 8</b>	-1.53E-05	15.19	54.08%	90.24%	81.25%
<b>Model 9</b>	-1.57E-05	15.01	80.28%	94.38%	85.52%

AIC: Akaike Information Criterion, RMSE: Root Mean Square Error

Table 3 – Regressors for each output for Model 9

Output	Regressors	Wavelet network (# units)
<b>Carbon capture rate</b>	Carbon capture (t-1, t-2, t-3), lean solvent CO <sub>2</sub> loading (t-1, t-2, t-3), total equivalent work (t-1, t-2, t-3), flue gas flowrate (t,t-1,t-2), lean solvent flowrate (t,t-1,t-2), steam flowrate (t,t-1,t-2)	6
<b>Lean solvent CO<sub>2</sub> loading</b>	Carbon capture(t-1, t-2, t-3), lean solvent CO <sub>2</sub> loading (t-1, t-2), total equivalent work (t-1, t-2, t-3, t-4), flue gas flowrate (t,t-1,t-2), lean solvent flowrate (t,t-1,t-2), steam flowrate (t,t-1,t-2)	10
<b>Total equivalent work</b>	Carbon capture(t-1, t-2, t-3, t-4), lean solvent CO <sub>2</sub> loading (t-1, t-2, t-3, t-4), total equivalent work (t-1, t-2, t-3, t-4), flue gas flowrate (t,t-1,t-2), lean solvent flowrate (t,t-1,t-2), steam flowrate (t,t-1,t-2)	8

In summary, the reduced-order CCS model is a dynamic NARX system composed of 3 inputs as decision variables, in which the flue gas flowrate is constrained, and 3 outputs as dependent variables, without cross-term variables. The CO<sub>2</sub> capture rate has 18 regressors, the lean solvent CO<sub>2</sub> loading has 18 regressors, and the total equivalent work has 21 regressors. The regressors are composed of past inputs and outputs. The general NARX model as well as the parameter values for each output can be found in the Supplementary material. The system is also bounded by the data range used for the system identification, as there is no guarantee that the identified NARX system is valid outside the selected data range.

#### 4.2. Optimization Formulation and Results

The optimization is performed using the MOO-DRTO proposed framework. The search space for the optimal solution is considered the same as the input ranges for the system identification in Equations (17) – (19). Moreover, there is the time constraint for the load-following scenario, in which the output optimal trajectories should be available in a timely manner to be implemented, i.e., the computational time cannot surpass the simulated optimization horizon.

Regarding the optimization formulation, economic and environmental objectives are defined in Equations (21) and (22). The economic objective aims to minimize the economic cost, meaning that the lower the economic objective value, the more improved is the economic objective, while the environmental objective aims to maximize the amount of carbon captured.

$$\min ECON(\Phi_1) = \Delta t \sum_t (E + Tr + S - CCred + Ctax - EOR) \quad (21)$$

$$\max ENV(\Phi_2) = \Delta t \sum_t (Carbon\ Captured) \quad (22)$$

in which,  $\Delta t$  is the discretization time step of 14.4s (0.004h). Regarding the economic objective,  $E$  is the energy penalty to capture carbon based on electricity price market and the extracted steam flowrate,  $Tr$  is the cost related to CO<sub>2</sub> transportation, such as onshore/off-shore and length of pipelines, and  $S$  is the cost related to CO<sub>2</sub> storage, such as onshore/off-shore and reuse of wells. Moreover, for carbon policies,  $CCred$  is the value for the carbon captured in a potential *cap&trade* scenario,  $Ctax$  is the tax embedded in the carbon released into the atmosphere, and  $EOR$  is the credit due to CO<sub>2</sub> utilization for enhanced oil recovery. Regarding the environmental objective, *Carbon Captured* is the CO<sub>2</sub> capture rate in Equation (15). As a remark, the developed framework could be easily adapted to simulate and assess the effect of different implementations of carbon policies such as the Policy 45Q<sup>(29)</sup>. Recommended values for the costs/credits associated with  $Tr$ ,  $S$  and  $EOR$  are obtained from the literature<sup>(30)</sup>.

As this study includes costs related to the carbon capture system, all cost values are scaled considering the 2017 Chemical Engineering Plant Cost Index (CEPCI)<sup>(31)</sup> and normalized to the same basis chosen as year 2000, to adjust transport and storage costs to 2017 inflation, as shown in Equation (23).

$$Cost_{2017} = Cost_{ref} * \frac{CEPCI_{2017}}{CEPCI_{ref}} \quad (23)$$

Specifically, the terms in the objective function are further defined in Equations (24) – (29):

$$E = x_3 * m_1 * EMP * t_1 \quad (24)$$

$$Tr = x_1 * y_1 * m_2 * t_1 \quad (25)$$

$$S = x_1 * y_1 * m_3 * t_1 \quad (26)$$

$$CCred = CCmarket * x_1 * y_1 * t_1 \quad (27)$$

$$Ctax = m_{4,TAX} * x_1^2 * (1 - y_1) * t_1 \quad (28)$$

$$EOR = m_5 * x_1 * y_1 * t_1 \quad (29)$$

in which  $y_1$  is the CO<sub>2</sub> capture rate. The  $m_l$  is the estimated value<sup>(32)</sup> for the equivalent generated electricity per ton of steam (kwh/kmol),  $m_2$  is the recommended<sup>(30)</sup> cost for onshore CO<sub>2</sub> transportation pipelines (2017 US\$/ton CO<sub>2</sub>/250km),  $m_3$  is the recommended<sup>(30)</sup> cost for onshore CO<sub>2</sub> storage (2017 US\$/ton CO<sub>2</sub>),  $m_{4,TAX}$  is the tax value imposed to the amount of carbon released (2017 US\$/ton CO<sub>2</sub>) based on existing similar policies<sup>(33)</sup>, and  $m_5$  is the recommended<sup>(30)</sup> value for EOR according to the amount of carbon captured (2017 US\$/ton CO<sub>2</sub>). Also,  $EMP$  is the electricity market price range (US\$/kwh). For this study, the hourly aggregate prices and grid load of the coal-fired power plant were obtained from the PJM Regional Transmission Organization<sup>(34)</sup>. More specifically, the aggregate load and electricity price of the entire region for 24 hours on March 30<sup>th</sup>, 2018 were used. As the framework considers the aggregate load and electricity price as forcing functions, these functions could be easily substituted to represent a specific node or power plant.  $CCmarket$  is the hypothetical change in the market price value of the CO<sub>2</sub> credit according to the amount of carbon captured (US\$/ton CO<sub>2</sub>) and  $t_1$  refers to the optimization horizon interval(s).

For the performed case studies, there is an underlying assumption that the flue gas flowrate is proportional to the power demand cycling profile. The assumed flue gas cycling,  $CCmarket$  and  $EMP$  curves throughout the considered time horizon are shown in Figure 5. The variability of the  $CCmarket$  function was assumed to change hourly, similar to the  $EMP$  trend, considering a potential

large-scale deployment scenario of the carbon credit system. The reason for introducing this variability is to evaluate the optimizer performance under the challenging conditions that this scenario would represent. Also, when the carbon captured is not sold for EOR, the economic objective accounts for storage costs. Otherwise, the related storage costs are not considered in the economic objective. The PSO parameters for both objectives in the optimization framework are  $\gamma = 1$ ,  $\Phi_1 = 2.05$ ,  $\Phi_2 = 2.05$ , maximum number of iterations = 3,  $v_{min}$  of  $x_2 = -0.0412$ ,  $v_{min}$  of  $x_3 = -0.0503$ ,  $v_{max}$  of  $x_2 = 0.0412$ ,  $v_{max}$  of  $x_3 = 0.0503$ . The population swarm for the economic objective is 50 and for the environmental objective is 40.

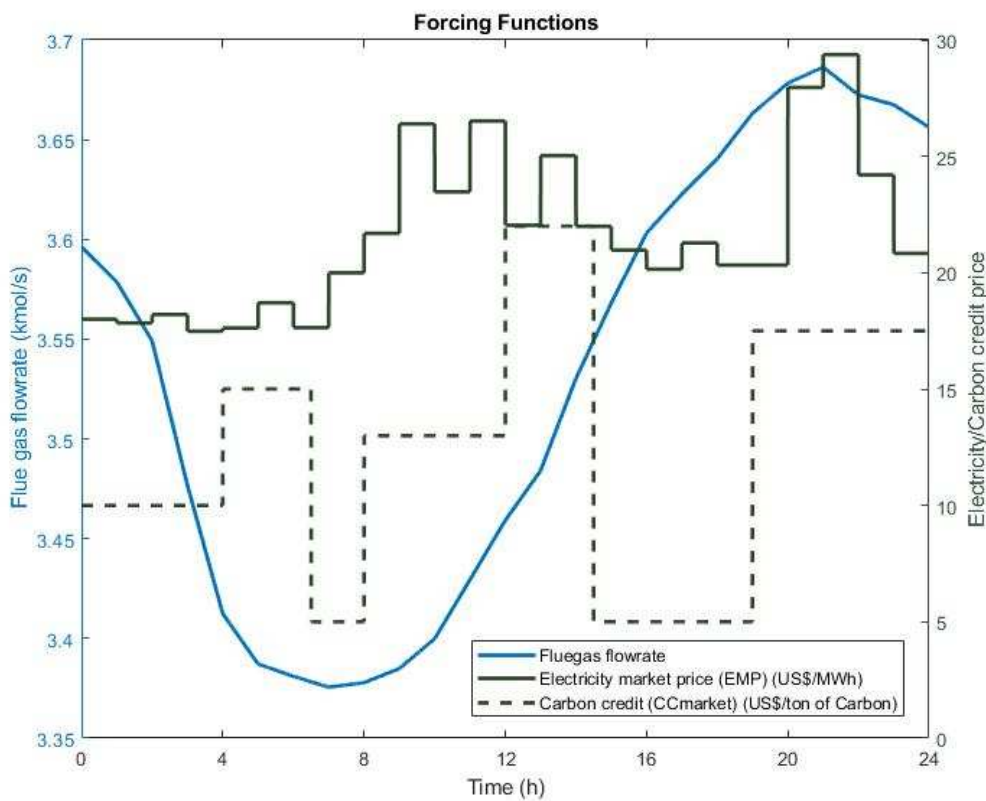


Figure 5 – Flue gas cycling profile (left axis), electricity market price (*EMP*) and carbon credit (*CCmarket*) (right axis) for 24-hour simulation horizon

Initially, a preliminary study is performed for the MOO component when selecting the optimal compromise with respect to different weight vectors. This study focuses on the first decision taken at  $t_0=0h$ , i.e.,  $T=1h$  and  $t_1=1h$ . For this preliminary study, the optimal compromise coordinates chosen for the MOO component are plotted against a previously mapped objective feasible space. After that, two case studies are presented, in which, optimal trajectories up to  $T=24h$  with  $t_1=1h$  are calculated considering different carbon capture policies.

Regarding the preliminary study for the decision at  $t_0=0h$ , the entire feasible space is first mapped offline using exhaustive search to delineate the Pareto Front (shown in blue in Figure 6). Then, weight values are uniformly changed and attributed in the Tchebycheff-based MOO formulation to assess the effect of this selection on the optimal compromise. The optimization for  $t_0=0h$  and  $T=1h$  is then performed using the MOO-DRTO framework. The CPU time to calculate each optimal compromise is within 120 to 180 seconds. The optimal compromises for the different weights (shown as red dots in Figure 6) are plotted and superimposed to the previously mapped feasible space. Also, all the values are scaled considering their respective positions to the offline mapping plotted which is also scaled using  $w_1= w_2=0.5$ .

As there are two objectives in this study,  $k=2$  and  $\sum_{i=1}^2 w_i = 1$ , there is only one degree of freedom to completely define the weight vector. The chosen increment from one weight vector to the other is 0.1, for instance, the first simulated point has  $w = [0, 1]$ , the subsequent simulated point has  $w = [0.1, 0.9]$  and so forth. From the analysis of Figure 6, the formulated MOO-DRTO is capable of choosing the compromise in the Pareto or very close to the Pareto front, within the set tolerances. Thus, as there is no need to compute the entire Pareto front, no computational time needs to be allocated to calculate the Pareto front to only choose one optimal compromise. Moreover, the optimal compromises are evenly distributed along the Pareto front as different weights are determined. The

constraint, step, and optimality difference tolerances as well as the maximum iterations used throughout the studies are shown in Table 4.

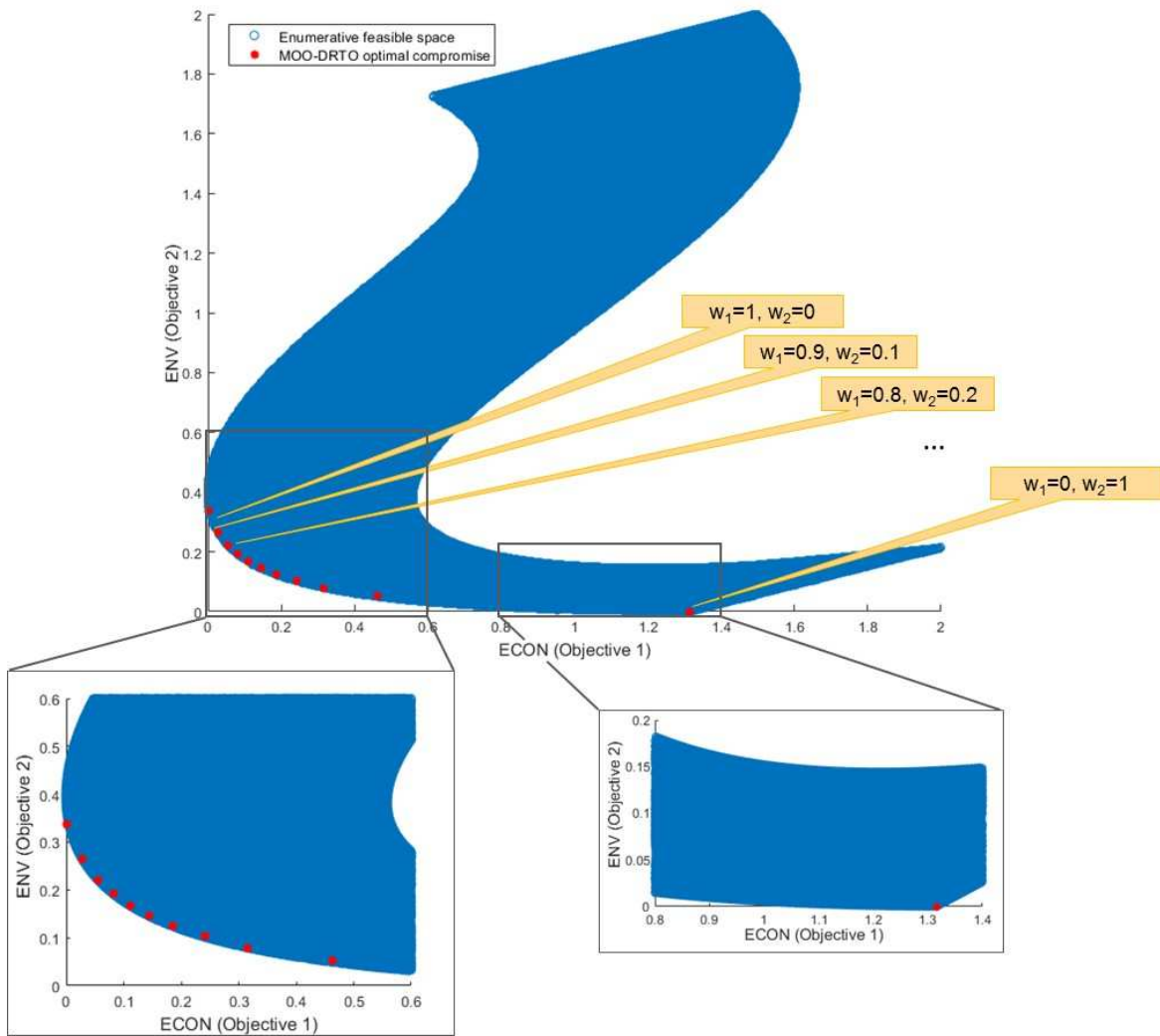


Figure 6 – Feasible space and distribution of optimal compromise for the first decision (t=0h, T=1h) and the optimal compromise according to the weight vector along the Pareto front

Table 4 – SQP tolerances for DRTO and MOO components

Parameters	SQP (DRTO)		SQP (MOO) – Modified and Traditional Tchebycheff
	Objective 1	Objective 2	
$C_{diff}$	1.00E-10	1.00E-10	1.00E-10
$O_{diff}$	1.00E-10	1.00E-16	1.00E-30
$S_{diff}$	1.00E-15	1.00E-15	1.00E-30
<b>Maximum Iterations</b>	500	500	1000

$C_{diff}$ : Constraint difference,  $O_{diff}$ : Optimality difference,  $S_{diff}$ : Step difference

Then, 24-hours trajectories are generated for the CCS using the MOO-DRTO framework. Two case studies are performed: Case 1 represents a scenario with absence of market for the captured CO<sub>2</sub> and absence of carbon tax policy. Case 2 represents a scenario with greater incentives for capturing carbon with available market for captured CO<sub>2</sub> as EOR and intermediate values for the carbon tax. The optimal compromise trajectories for both case studies, denoted as Case “number” - MOO, are determined using equal weights for the objectives, i.e.,  $w_1=w_2=0.5$ . Also, the optimization parameters for Case 1 are  $m_2 = 4.9$  (2017 US\$/ton CO<sub>2</sub>),  $m_3 = 13$  (2017 US\$/ton CO<sub>2</sub>),  $m_{4,TAX} = m_5 = 0$  (US\$/ton CO<sub>2</sub>), while for Case 2 are  $m_2 = 4.9$  (2017 US\$/ton CO<sub>2</sub>),  $m_3 = 13$  (2017 US\$/ton CO<sub>2</sub>),  $m_{4,TAX} = 30.01$  (US\$/ton CO<sub>2</sub>), and  $m_5 = 27.51$  (US\$/ton CO<sub>2</sub>). The optimal output trajectories generated are depicted in Figure 7. In this figure, the optimal output trajectories using  $w = [0, 1]$  and  $w = [1,0]$ , i.e., the single-objective optimizations of the case study are also shown, denoted as Case “number” - ECON and Case “number” - ENV for the economic and environmental objectives, respectively.

As shown in Figure 7, the optimal output trajectories for the single economic objective changes from case to case, as the economic incentives for carbon capture change, whereas the optimal output trajectories for the standalone environmental objective remain the same. The observed result is qualitatively expected as the economic terms are changing while the environmental objective is defined solely based on the capacity that the system has to physically capture carbon. Also, although

Case 2 represents an economic scenario to increase the amount of carbon captured, as seen in Case 2 – ECON in Figure 7, the generated Case 2 – ECON optimal trajectory considering only economic incentives is not equivalent to the Case 2 – ENV trajectory. This result emphasizes the importance of using a multi-objective strategy when it concerns objectives that cannot be directly monetized without altering the optimal trajectories.

Figure 7 (C, D) show that around  $t = 12\text{h}$  for the Cases 1 and 2 - ECON there is a sudden increase on the lean solvent  $\text{CO}_2$  loading for both case studies. The reason for this increase can be attributed to the changes in the forcing function profiles in Figure 5, in which there is an increase of the carbon credit value and a decrease of electricity price, along with a need to ramp up the CCS. This increase on the loading also affects the amount of work that the reboiler needs to exert to recover the MEA solvent, as seen in Figure 7 (E, F). Moreover, the peak in the lean solvent loading in Case 2 – ECON at  $t = 12\text{h}$  shown in Figure 7 – (D) is higher than the one in Case 1 – ECON in Figure 7 – (C), which causes the change in the total power consumption to be steeper in Case 2 – ECON in Figure 7 – (F) than in Case 1 – ECON in Figure 7 – (E).

As previously stated, no further interaction is required to calculate the optimal output trajectories after the objective weight is selected by the decision maker. Concerning the computational performance, the CPU time to simulate and calculate a 24-hour optimization horizon was around 45 to 60 minutes. As the elapsed time does not violate the time constraint by a large margin for a power plant load following scenario, the results indicate that the framework could be used in an online fashion and different optimization time horizons could be adopted. In addition to the optimal output trajectories, the mean of the hourly economic and environmental objectives data values are calculated and plotted, as shown in Figure 8.

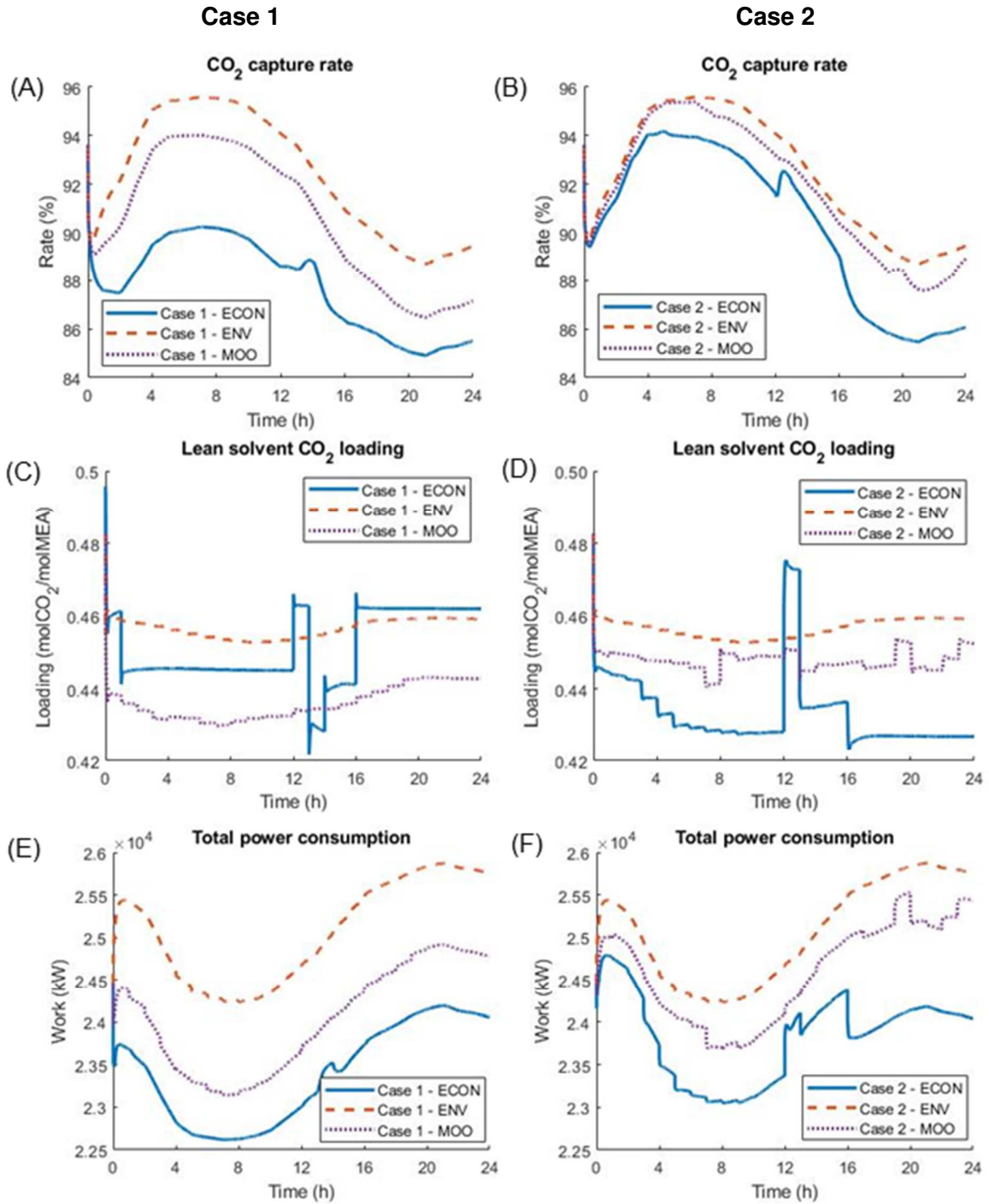


Figure 7 – CO<sub>2</sub> capture rate optimal (A, B), lean solvent CO<sub>2</sub> loading (C, D), and total equivalent work (E, F) profiles for Case 1 (left) and Case 2 (right)

Figure 8 (A, B) show the mean economic objective values per hour, i.e., the average hourly economic objective value over the 24-hour length of optimization. There are shift signs from Case 1 to Case 2,

as Case 2 has more advantageous economic policies to incentivize carbon capture. As previously asserted, the cost objective aims to minimize overall operating cost. When optimizing the environmental objective represented in Case 2 – ENV, the cost value is lower than the value obtained when optimizing the economic objective represented in Case 2 – ECON. This result can be attributed to the relationship of the forcing function profiles with the bound constraints imposed on the decision variables space of the system. For example, at early hours of Case 2 - ECON, the optimal decision is to maintain the system at a relatively lower carbon capture rate when compared to Case 2 – ENV. However, as the carbon credit increases and the flue gas flowrate decreases (see profiles in Figure 5), representing the penetration of the renewables into the grid, there is an opportunity to increase profit by capturing more carbon. In the attempt to increase the amount of carbon captured, the optimizer hits the upper bound of the decision variables for Case 2 - ECON and thus cannot reach higher values of capture rate, whereas for Case 2 – ENV, the system is already at a position of high values of carbon capture rate. One strategy that could be adopted to circumvent this issue would be to have a terminal constraint. Note that a synergistic effect can be detected in Case 2 – MOO, as the cost mean value is lower than those from the single objective optimizations. This effect is observed because the MOO-DRTO remains optimal considering both objectives. Thus, in this scenario, the optimizer is able to perform as Case 2 – ECON at early hours but also it is capable to ramp the system to higher capture rates similar to Case 2 – ENV, when the capture of carbon becomes advantageous.

Figure 8 (C, D) show the mean environmental objective value per hour, i.e., the average hourly environmental objective value over the 24-hour length of optimization. There is an overall increase of the carbon captured in Case 2 can be detected when compared to Case 1. The difference in monetary compensation for carbon capture does not affect the environmental objective standalone optimization. Such incentives, however, affect the economic objective standalone optimization, thus

changing the MOO-DRTO optimization result. In both cases, the mean environmental objective value of the MOO-DRTO remained in between the single-objective optimizations, with a higher mean capture rate in Case 2.

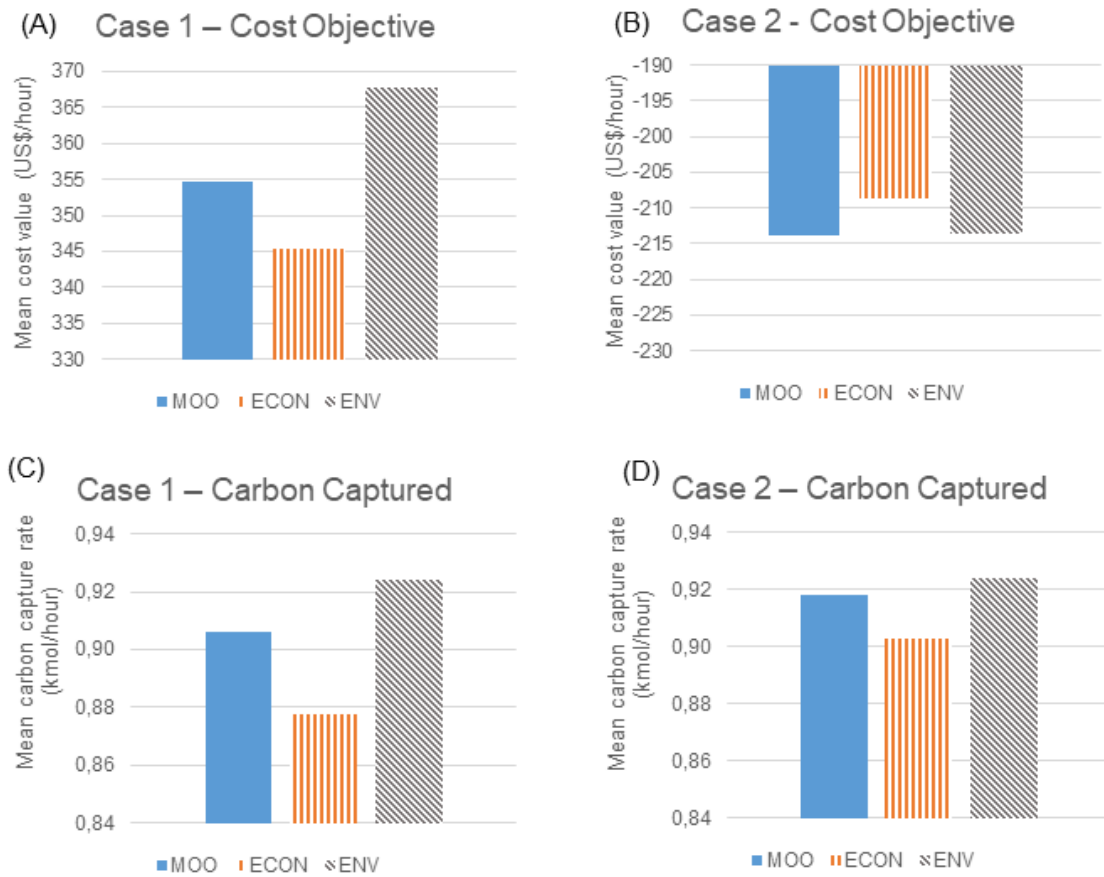


Figure 8 – Mean value for cost (A, B) and carbon captured (C, D) objectives for Case 1- and Case 2-MOO, ECON, ENV

## 5. Conclusions

In this work, a multi-objective and dynamic real-time optimization strategy was proposed and successfully implemented on a reduced-order model of a carbon capture process under cycling conditions considering economic and environmental objectives. The DRTO framework is based on a PSO and SQP hybrid algorithm and the MOO is based on the Tchebycheff method implemented using an SQP-based algorithm. The SQP used in the DRTO was augmented using the PSO to explore the entire feasible space, enabling a systematic definition of the initial guess for the SQP in the DRTO formulation. The Tchebycheff-method is able to select the Pareto optimal compromise without requiring the computation of the entire Pareto front.

Case studies were performed which assessed the influence of different carbon policies in the computation of optimal output trajectories. It was concluded that economic incentives increased the overall amount of carbon captured considering the economic objective, but the obtained trajectories were not equivalent to the ones calculated by an environmental objective optimization. A synergistic effect was also observed on the MOO-DRTO performance.

The novel optimization framework was formulated considering the time constraint to solve a dynamic problem and implemented on a chemical process. The proposed optimization framework could potentially ease the renewables intermittency effects on baseload processes. Optimal output trajectories of 24-hours for the baseload CCS under cycling were calculated with minimal interaction with the decision maker, which is desired for online implementation, and within the load-following time constraint. The results obtained indicate that the MOO-DRTO is a promising optimization alternative that could enhance the performance of baseload power plants under cycling.

## Acknowledgments

The authors gratefully acknowledge the financial support from U.S.-China Clean Energy Research Center (CERC) program and U.S. Department of Energy under Cooperative Agreement DEPI0000017.

## Notation

$c_1, c_2$  – Cognitive and social acceleration coefficients

$CCred$  – Carbon credit in cap&trade scenario

$CCmarket$  – Hypothetical change in the market price value of the CO<sub>2</sub> credit

$Ctax$  – Tax for the carbon released into the atmosphere

$E$  – Energy penalty cost for the carbon capture based on electricity price market and steam flowrate

$f$  – Dynamic system model

$F$  – Decision space

$fc$  – Nonlinear mapping

$g$  – Equality constraints

$h$  – Inequality constraints

$IT$  – Inertia term

$m_1$  – Equivalent generated electricity per ton of steam

$m_2$  – Cost for onshore CO<sub>2</sub> transportation pipelines

$m_3$  – Cost for onshore CO<sub>2</sub> storage

$m_{4,TAX}$  – Tax value imposed to the amount of carbon released

$m_5$  – Enhanced oil recovery (EOR) value

$n_y, n_u$  – Maximum input and output lags

$p_j$  – Position of the j-th particle

$PB_j$  – Personal best position of the j-th particle

$r_1, r_2$  – Random numbers

$SB$  – Swarm best position

$S$  – CO<sub>2</sub> storage cost

$t$  – Time

$t_1$  – Optimization time horizon interval

$Tr$  – CO<sub>2</sub> transportation cost

$T$  – Optimization time horizon

$u$  – Input variables for the system identification

$v_j$  – Velocity of the j-th particle

$y_4$  – CO<sub>2</sub> capture rate

$w_i$  – Tchebycheff weight vector

$x$  – Decision variables

$x_1$  – Flue gas flowrate

$x_3$  – Steam flowrate

$y$  – Model output

$z^0$  – Ideal vector

### *Acronyms*

AIC – Akaike Information Criterion

CFPP – Coal-fired power plant

CCS – Carbon capture system

CEPCI - Chemical Engineering Plant Cost Index

DCC – Direct contact cooler

DRTO – Dynamic real-time optimization

EOR – Enhanced oil recovery

EMP – Electricity market price range

IPCC – Intergovernmental Panel on Climate Change

NGPP – Natural gas-fired power plant

MEA – Monoethanolamine

MOO – Multi-objective optimization

MOO-DRTO – Multi-objective and dynamic real-time optimization

MTch – Modified Tchebycheff

NARX – Nonlinear autoregressive with exogenous inputs

PSE – Process systems engineering

PSO – Particle swarm optimization

RMSE – Root mean square error

ref – Reference

SCPC – Supercritical pulverized coal-fired power plant

SQP – Sequential quadratic programming

SS – Steady state

*Tch* – Tchebycheff

*Greek letters*

$\Delta t$  – Discretization time interval

$\gamma, \Omega, \Omega_1, \Omega_2$  - PSO constriction factor method parameters

$\varepsilon$  – Independent identically distributed random variable

$\Phi$  – Objective function

## Literature Cited

- (1) U.S. Energy Information Administration. “Annual Energy Outlook”. Link: <https://www.eia.gov/outlooks/aeo/pdf/AEO2018.pdf>. Accessed on: November 14<sup>th</sup>, 2018.
- (2) Blazquez, J., Fuentes-Bracamontes, R., Bollino, C. A. and Nezamuddin, N. (2018) “The Renewable Energy Policy Paradox,” *Renewable and Sustainable Energy Reviews: Part 1*, 82, pp. 1–5. doi: 10.1016/j.rser.2017.09.002.
- (3) Raimi, D. (2017) “Decommissioning US Power Plants. Decisions, Costs and Key Issues”. *Resources for the Future*.
- (4) Nalbandian-Sugden, H. (2016) “Operating ratio and cost of coal power generation”. IEA Clean Coal Centre.
- (5) Houser, T., Bordoff, J., Marsters, P. (2017) “Can Coal Make a Comeback?”. Columbia SIPA, Center on Global Energy Policy.
- (6) Bentek Energy LLC. (2010) “How less became more... Wind, Power and Unintended Consequences in the Colorado Energy Market”.
- (7) National Energy Technology Laboratory - NETL. (2015) “Impact of Load Following on the Economics of Existing Coal-Fired Power Plant Operations”. DOE/NETL – 2015/1718
- (8) National Renewable Energy Laboratory – NREL. (2009) “Wind Plant Ramping Behavior”. *Technical Report* NREL/TP-550-46938
- (9) Biegler L.T (2014) “Nonlinear Programming Strategies for Dynamic Chemical Process Optimization,” *Theoretical Foundations of Chemical Engineering*, 48(5), pp. 541–554. doi: 10.1134/S0040579514050157.

- (10) Trifkovic, M., Marvin, W. A., Daoutidis, P. and Sheikhzadeh, M. (2014) “Dynamic Real-Time Optimization and Control of a Hybrid Energy System,” *AIChE Journal*, 60(7), pp. 2546–2556. doi: 10.1002/aic.14458.
- (11) Jamaludin, M. Z. and Swartz, C. L. E. (2017) “Dynamic Real-Time Optimization with Closed-Loop Prediction,” *AIChE Journal*, 63(9), pp. 3896–3911. doi: 10.1002/aic.15752.
- (12) Bankole, T., Jones, D., Bhattacharyya, D., Turton, R. and Zitney, S. E. (2018) “Optimal Scheduling and Its Lyapunov Stability for Advanced Load-Following Energy Plants with CO<sub>2</sub> Capture,” *Computers and Chemical Engineering*, 109, pp. 30–47. doi: 10.1016/j.compchemeng.2017.10.025.
- (13) Dowell, N. M. and Shah, N. (2014) “Optimisation of Post-Combustion CO<sub>2</sub> Capture for Flexible Operation,” *Energy Procedia*, 63, pp. 1525–1535.
- (14) Intergovernmental Panel on Climate Change – IPCC. (2018). Summary for Policymakers. In: Global warming of 1.5°C. An IPCC Special Report on the impacts of global warming of 1.5°C above pre-industrial levels and related global greenhouse gas emission pathways, in the context of strengthening the global response to the threat of climate change, sustainable development, and efforts to eradicate poverty [V. Masson-Delmotte, P. Zhai, H. O. Pörtner, D. Roberts, J. Skea, P.R. Shukla, A. Pirani, W. Moufouma-Okia, C. Péan, R. Pidcock, S. Connors, J. B. R. Matthews, Y. Chen, X. Zhou, M. I. Gomis, E. Lonnoy, T. Maycock, M. Tignor, T. Waterfield (eds.)]
- (15) Zhang, Q., Turton, R. and Bhattacharyya, D. (2016) “Development of Model and Model-Predictive Control of an Mea-Based Postcombustion CO<sub>2</sub> Capture Process” *Industrial & Engineering Chemistry Research*, 55(5), pp. 1292–1308. doi: 10.1021/acs.iecr.5b02243.

- (16) He, X., Wang, Y., Bhattacharyya, D., Lima, F. V. and Turton, R. (2018) “Dynamic Modeling and Advanced Control of Post-Combustion CO<sub>2</sub> Capture Plants,” *Chemical Engineering Research and Design*, 131, pp. 430–439. doi: 10.1016/j.cherd.2017.12.020.
- (17) He, X. and Lima, F. V. (2019) “Development and Implementation of Advanced Control Strategies for Power Plant Cycling with Carbon Capture,” *Computers and Chemical Engineering*, 121, pp. 497–509. doi: 10.1016/j.compchemeng.2018.11.004
- (18) Diwekar, U. M. (2008). “Introduction to Applied Optimization”. 2nd edn. New York: Springer (Springer Optimization and its Applications, v. 22).
- (19) Coello Coello, C. A., Lamont, G. B. and Van Veldhuisen, D. A. (2007) “Evolutionary algorithms for solving multi-objective problems”. 2nd edn. New York: Springer (Genetic and evolutionary computation series).
- (20) Brownlee, J. *Clever Algorithms: Nature-Inspired Programming Recipes*. <http://www.cleveralgorithms.com/nature-inspired/swarm/pso.html>. Accessed on September 2018.
- (21) Sengupta, S., Basak, S., and Peter II, R.A. (2018) “Particle Swarm Optimization: A survey of historical and recent developments with hybridization perspectives”. Cornell University Library Arxiv, Neural and Evolutional Computing. Available at <https://arxiv.org/abs/1804.05319>. Accessed on December 2018.
- (22) Elaiw, A. M., Xia, X. and Shehata, A. M. (2013) “Hybrid DE-SQP and Hybrid PSO-SQP Methods for Solving Dynamic Economic Emission Dispatch Problem with Valve-Point Effects,” *Electric Power Systems Research*, 103, pp. 192–200.

- (23) Ma, X., Zhang, Q., Tian, G., Yang, J., Zhu, Z. (2018) “On Tchebycheff Decomposition Approaches for Multiobjective Evolutionary Optimization” *IEEE Transactions on Evolutionary Computation*, 22, pp. 226–244.
- (24) National Energy Technology Laboratory – NETL (2015) “Cost and Performance Baseline for Fossil Energy Plants Volume 1a: Bituminous Coal (PC) and Natural Gas to Electricity”. DOE/NETL – 2015/1723
- (25) U.S. Energy Information Administration – EIA. (2013). “Further Sensitivity Analysis of Hypothetical Policies to Limit Energy-Related Carbon Dioxide Emissions”. *Supplement to the Annual Energy Outlook 2013*.
- (26) Bhattacharyya D., Rengaswamy R. (2010) “System Identification and Nonlinear Model Predictive Control of a Solid Oxide Fuel Cell,” *Industrial and Engineering Chemistry Research*, 49(10), pp. 4800–4808. doi: 10.1021/ie9020254.
- (27) Pearson, R. K. (1999) “Discrete-time dynamic models”. New York: Oxford University Press (Topics in chemical engineering). Available at:  
<http://public.ebib.com/choice/publicfullrecord.aspx?p=431187>. Accessed on: April 2018.
- (28) Wei, H. L., Billings, S. A. and Balikhin, M. A. (2003) “Wavelet Based Nonparametric NARX Models for Nonlinear Input-Output System Identification”, *Research Report No 831*.
- (29) Future Act S.1535 – 115<sup>th</sup> Congress (2017-2018). Available at:  
“<https://www.congress.gov/bill/115th-congress/senate-bill/1535/text>”. Accessed on January 2019

- (30) Rubin, E. S., Davison, J. E. and Herzog, H. J. (2015) “The Cost of CO<sub>2</sub> Capture and Storage”. *International Journal of Greenhouse Gas Control*, 40, pp. 378–400. doi: 10.1016/j.ijggc.2015.05.018.
- (31) Chemical Engineering Magazine. Chemical Engineering Plant Cost Index. Available at: “[www.chemengonline.com/pci](http://www.chemengonline.com/pci)”. Accessed on October 2018.
- (32) Global CCS Institute. Available at: “<https://hub.globalccsinstitute.com/publications/adb-technical-assistance-project-aspen-simulation-and-evaluation-economic-feasibility-co2-capture-gaojing-gas-fired-power-plant/53-operating-costs>”. Accessed on October 2017.
- (33) Carbon Tax Center. Available at: “[www.carbontax.org/where-carbon-is-taxed/](http://www.carbontax.org/where-carbon-is-taxed/)”. Accessed on October 2017
- (34) PJM. Available at: <http://www.pjm.com/markets-and-operations/ops-analysis.aspx>. Accessed on June 2018.

